p90 ribosomal S6 kinase 2 promotes invasion and metastasis of human head and neck squamous cell carcinoma cells

Sumin Kang,[1] Shannon Elf,[1] Katherine Lythgoe,[1] Taro Hitosugi,[1] Jack Taunton,[2] Wei Zhou,[1] Li Xiong,[3] Dongsheng Wang,[1] Susan Muller,[4] Songqing Fan,[1] Shi-Yong Sun,[1] Adam I. Marcus,[1] Ting-Lei Gu,[5] Roberto D. Polakiewicz,[5] Zhuo (Georgia) Chen,[1] Fadlo R. Khuri,[1] Dong M. Shin,[1] and Jing Chen[1]

[1]Winship Cancer Institute of Emory University, Atlanta, Georgia. [2]Howard Hughes Medical Institute, Department of Cellular and Molecular Pharmacology, University of California, San Francisco. [3]Department of Mathematics and Computer Science and [4]Department of Pathology and Laboratory Medicine, Emory University, Atlanta, Georgia. [5]Cell Signaling Technology Inc. (CST), Danvers, Massachusetts.

Head and neck squamous cell carcinoma (HNSCC) is one of the most common types of human cancer and frequently metastasizes to LNs. Identifying metastasis-promoting factors is of immense clinical interest, as the prognosis for patients with even a single unilateral LN metastasis is extremely poor. Here, we report that p90 ribosomal S6 kinase 2 (RSK2) promotes human HNSCC cell invasion and metastasis. We determined that RSK2 was overexpressed and activated in highly invasive HNSCC cell lines compared with poorly invasive cell lines. Expression of RSK2 also correlated with metastatic progression in patients with HNSCC. Ectopic expression of RSK2 substantially enhanced the invasive capacity of HNSCC cells, while inhibition of RSK2 activity led to marked attenuation of invasion in vitro. Additionally, shRNA knockdown of RSK2 substantially reduced the invasive and metastatic potential of HNSCC cells in vitro and in vivo in a xenograft mouse model, respectively. Mechanistically, we determined that cAMP-responsive element-binding protein (CREB) and Hsp27 are phosphorylated and activated by RSK2 and are important for the RSK2-mediated invasive ability of HNSCC cells. Our findings suggest that RSK2 is involved in the prometastatic programming of HNSCC cells, through phosphorylation of proteins in a putative signaling network. Moreover, targeting RSK2 markedly attenuates in vitro invasion and in vivo metastasis of HNSCC cells, suggesting that RSK2 may represent a therapeutic target in the treatment of metastatic HNSCC.

Introduction

Metastasis continues to be the cause of more than 90% of human cancer deaths. However, how tumors spread and kill their host organism remains an enigma. Current underlying concepts hypothesize that metastatic tumor cells emerge from the somatic evolution of a population of cancer cells that are genetically diversified due to selective pressures from the microenvironment. Only a very small population of these cancer cells will achieve the ability to colonize a distant organ when released into the circulation. In addition, these metastatic cells must evade multiple barriers that are posed by healthy tissues to successfully complete invasion and colonization. Thus, metastasis likely represents an evolutionary process that involves selection of genetically heterogeneous lineages of cancer cells within the context of a whole organism (1, 2). Metastasis is a biological cascade of multiple steps: loss of cellular adhesion, increased motility and invasiveness, entry and survival in the circulation, exit into new tissue, and eventual colonization at a distant site. This suggests that cells containing metastatic lesions would have to accumulate expression of multiple, if not all, genes necessary for successful execution of the metastatic cascade from the primary tumor (3). Therefore, important and long-standing questions that remain concern the identity of genes that mediate these metastasis-promoting processes. Identification and characterization of these genes will not only shed new insight into the molecular basis

of cancer metastasis but also inform therapeutic strategies to improve the outcome of treatment of human cancers.

Head and neck squamous cell carcinoma (HNSCC) is one of the most common types of human cancer, with an annual incidence of more than 500,000 cases worldwide. Although recent molecular studies have advanced our understanding of the disease and provided a rationale to develop novel therapeutic strategies, HNSCC is still associated with severe disease- and treatment-related morbidity, with a 5-year survival rate of only approximately 50%, which has not improved in more than 30 years (4). Worse yet, the 5-year survival rate is even lower for HNSCC patients with a single unilateral LN metastasis (LNM) and less than 25% for patients with bilateral LNM. Current clinical treatments of HNSCC include surgery, radiotherapy, chemotherapy, and molecularly targeted agents. As with most forms of cancer, treatment of HNSCC depends largely on tumor stage. The detection of local LNM is pivotal for choosing appropriate treatment, especially for individuals diagnosed with HNSCC in the oral cavity or oropharynx. However, distant metastasis from HNSCC to lung or bone usually represents incurable disease. Therefore, it is of clinical interest to identify metastasis-promoting genes in primary HNSCC tumors to improve prognosis and define targets for therapy.

Protein kinases have been implicated in mediating prometastatic signaling in human cancers. For example, the hERBB2 receptor tyrosine kinase is overexpressed in 30% of cases of primary human breast cancer, which correlates with tumor progression and poor patient outcome (5). We began addressing this issue by examining correlations between the expression of protein kinases and
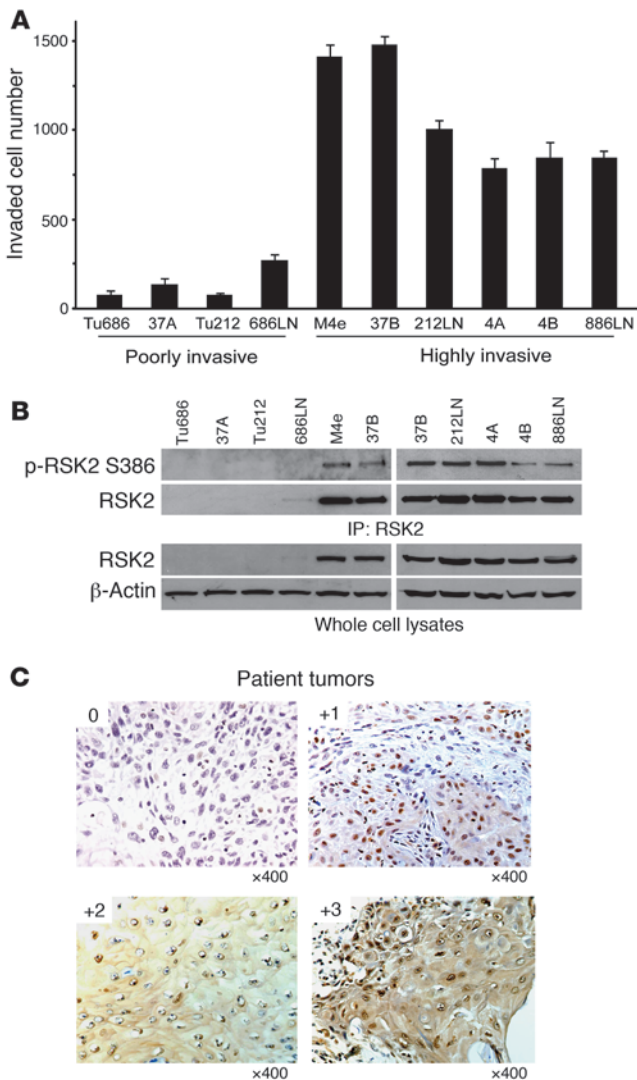
Figure 1

RSK2 is overexpressed in a group of highly invasive human HNSCC metastatic cell lines, and the pattern of RSK2 expression correlates with HNSCC cancer progression. (**A**) In vitro Matrigel invasion assay demonstrates differential invasive ability of diverse human HNSCC cell lines that are divided into 2 groups, including a poorly invasive group that includes Tu686, 37A, Tu212, and 686LN and a highly invasive group that includes M4e, 37B, 212LN, 4A, 4B, and 886LN (mean ± SD). (**B**) RSK2 expression correlates with the invasive ability of diverse HNSCC cells. RSK2 was overexpressed and activated in cell lines of the highly invasive group (M4e, 37B, 212LN, 4A, 4B, and 886LN) compared with cell lines in the poorly invasive group (Tu686, 37A, Tu212, and 686LN). (**C**) Representative IHC staining images are shown for 0, 1+, 2+, and 3+ scores of human metastatic HNSCC tissue samples. Original magnification, ×400.

metastasis-promoting signaling network by activating multiple signaling effectors that subsequently potentiate the invasive and metastatic abilities of HNSCC cells.

Herein, we report that continued RSK2 expression contributes to the maintenance of the invasive and metastatic potential of HNSCC cells and that the pattern of RSK2 expression correlates with HNSCC cell invasive ability as well as human head and neck cancer progression. Moreover, we also identified multiple prometastatic protein factors whose phosphorylation and activation levels are regulated by RSK2, including the known RSK2 substrate, CREB, and a newly identified RSK2 substrate, Hsp27. These findings suggest that RSK2 programs a prometastatic signaling network in HNSCC cells.

Results

RSK2 expression correlates with cell invasive ability of diverse human HNSCC cell lines and HNSCC progression. We performed an in vitro Matrigel invasion assay, using diverse human HNSCC cell lines. Based on the differential invasive ability, these cell lines were divided into 2 groups: a poorly invasive group that includes Tu686, 37A, Tu212, and 686LN and a highly invasive group that includes M4e, 37B, 212LN, 4A, 4B, and 886LN (Figure 1A). We found that RSK2 was overexpressed and activated, as assessed by phosphorylation at Ser386, in the highly invasive cell lines, including M4e, 37B, 212LN, 4A, 4B, and 886LN, compared with the poorly invasive cell

the tumor progression of head and neck cancer. We found that p90 ribosomal S6 kinase 2 (RSK2) is predominantly expressed in a spectrum of metastatic human HNSCC cell lines, compared with the parental, poorly metastatic cells. RSK family members share structural and functional similarities and contain 2 distinct kinase domains, both of which are catalytically functional (reviewed in refs. 6, 7). The C-terminal kinase domain (CTD) is responsible for autophosphorylation at Ser386 (numbering based on the murine RSK2 amino acid sequence) that is critical in RSK activation, whereas the N-terminal kinase domain (NTD) is believed to phosphorylate exogenous substrates of RSK. RSK phosphorylates multiple signaling effectors to play an essential role in a number of cellular functions, including regulation of gene expression by phosphorylation of transcriptional regulators, including c-Fos and cAMP-responsive element-binding protein (CREB) (8), as well as phosphorylation of histone H3 (9), which contributes to the chromatin remodeling during mitosis and transcriptional activation; regulation of cell cycle by phosphorylating and inhibiting Myt1 (10), a p34^{cdc2} inhibitory kinase in *Xenopus* extracts; and regulation of cell survival by phosphorylating BAD (11), Bim (12), and death-associated protein (DAP) kinase (13) to protect cells from apoptosis. Therefore, RSK2 may serve as a key regulator in the

Table 1

IHC analysis of primary tissue samples from patients with HNSCC

IHC signal intensity (0–3+)	Primary tissue samples from HNSCC patients		
	Tu^{-Met} (no. patients)	Tu^{+Met} (no. patients)	LN^{+Met} (no. patients)
0	39	26	19
1+	8	17	21
2+	3	7	10
3+	1	1	0
Total sample no.	51	51	50
RSK2 positive	24%	49%	62%
		$P = 0.007$	$P < 0.0001$

RSK2 expression pattern correlates with HNSCC cancer progression. IHC analysis was performed using a group of primary patient tissue specimens, including 51 Tu^{-Met}, 51 Tu^{+Met}, and 50 LN^{+Met} samples. The P values were determined by χ^2 test.
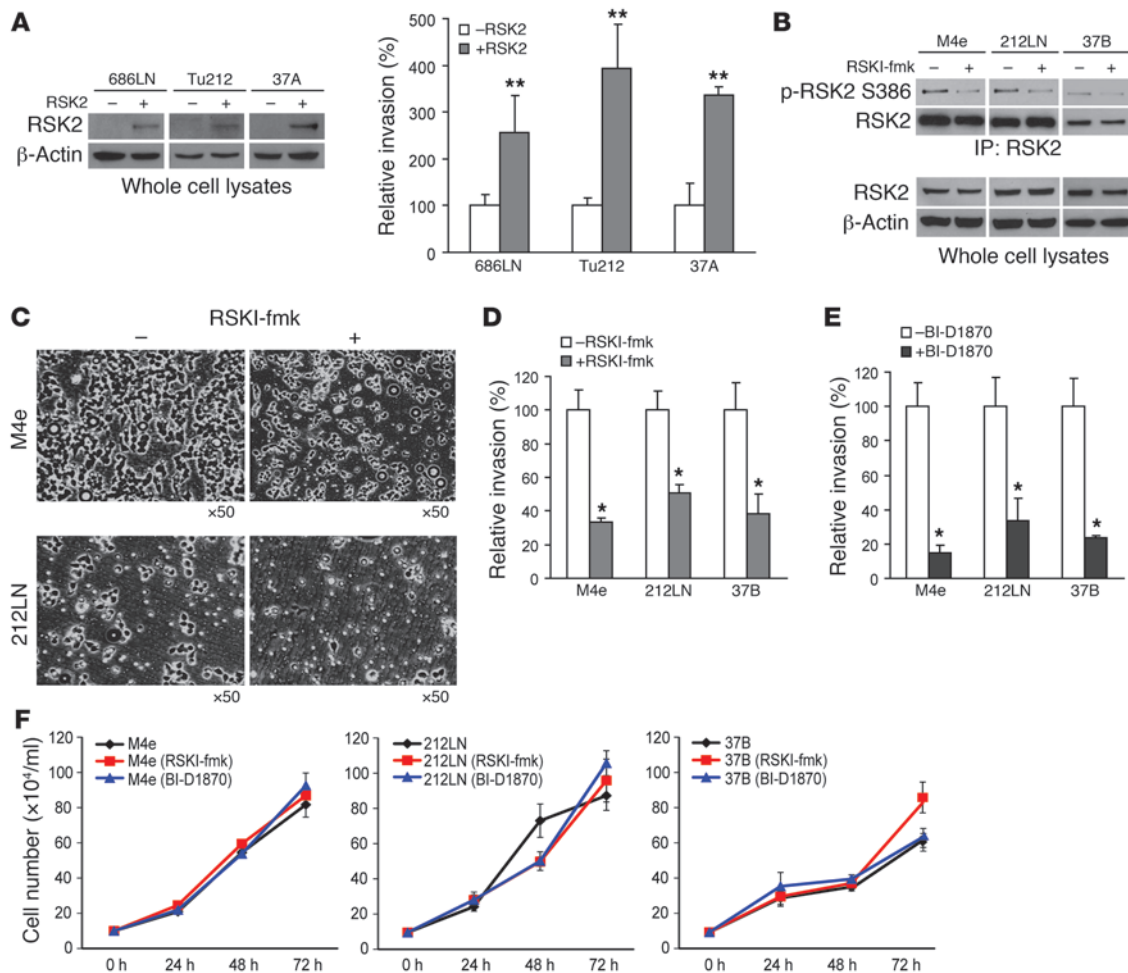
Figure 2
Expression of RSK2 promotes in vitro HNSCC cell invasion. (**A**) Enforced expression of RSK2 resulted in increased invasive ability in poorly metastatic HNSCC cells, including 686LN, Tu212, and 37A, in the in vitro Matrigel invasion assay. Relative invasion was normalized to the invasion of control cells without transfection (mean ± SD). **$P < 0.01$, by 2-tailed Student's t test. (**B**) Treatment with RSKI-fmk (6 μM) effectively decreased RSK2 kinase activity, as assessed by phosphorylation level of S386, in RSK2-expressing M4e, 212LN, and 37B cells. (**C**) Representative areas show that inhibition of RSK2 by RSKI-fmk treatment decreased the numbers of M4e and 212LN cells that crossed the Matrigel in the invasion assay. Original magnification, ×50. (**D** and **E**) Inhibition of RSK2 by RSKI-fmk (**D**) or BI-D1870 (**E**) (6 μM) decreased invasive ability of M4e, 212LN, and 37B cells. Relative invasion was normalized to the invasion of control cells without drug treatment (mean ± SD; *$P = 0.01–0.05$). (**F**) Targeting RSK2 by RSKI-fmk or BI-D1870 (6 μM) did not significantly affect the proliferation rate of M4e, 212LN, and 37B cells (mean ± SD). Cell number of each sample was determined by normalizing the cell viability to that of a standard curve of cell number.

lines, including Tu686, 37A, Tu212, and 686LN (Figure 1B). These data suggest that RSK2 expression may promote HNSCC cell invasion and tumor metastasis.

We next conducted a study to detect RSK2 expression by an immunohistochemistry (IHC) assay, using primary human HNSCC patient tissue samples. We first characterized the RSK2 antibody (Novus Biologicals) using RSK2-negative Tu212 cells and RSK2-positive 212LN cells that were embedded in paraffin (Supplemental Figure 1A; supplemental material available online with this article; doi:10.1172/JCI40582DS1). Positive Western blot and IHC staining of RSK2 was observed in 212LN cells but not in Tu212 cells. Moreover, we evaluated this antibody using primary tumor tissue samples from xenografted mice injected with either control M4e-pLKO.1 cells or M4e-pLKO.1-RSK2 shRNA cells with stable knockdown of RSK2 (described below). Positive Western blot and IHC staining of

RSK2 was observed in tumor tissue samples derived from control M4e-pLKO.1 cells but not in those from M4e-pLKO.1-RSK2 shRNA cells (Supplemental Figure 1B).

Tumor and LN specimens representing 3 categories were evaluated, including primary tumors from patients with nonmetastatic disease (Tu^{-Met}), primary tumors from patients with metastatic HNSCC (Tu^{+Met}), and paired metastatic LN (LN^{+Met}) samples from the same patients. As shown in Figure 1C, positive staining of RSK2 was determined by the IHC signal intensity (scored as 0–3+) in the cytoplasm in a percentage of tumor cells. Table 1 presents the summarized data, with statistical analysis showing that the percentages of RSK2-positive cases (scored 1+, 2+, or 3+) are significantly higher in the paired tissue samples of primary tumor (Tu^{+Met}) and metastatic LNs (LN^{+Met}) from patients with metastatic HNSCC than the primary tumor specimens (Tu^{-Met}) from patients with
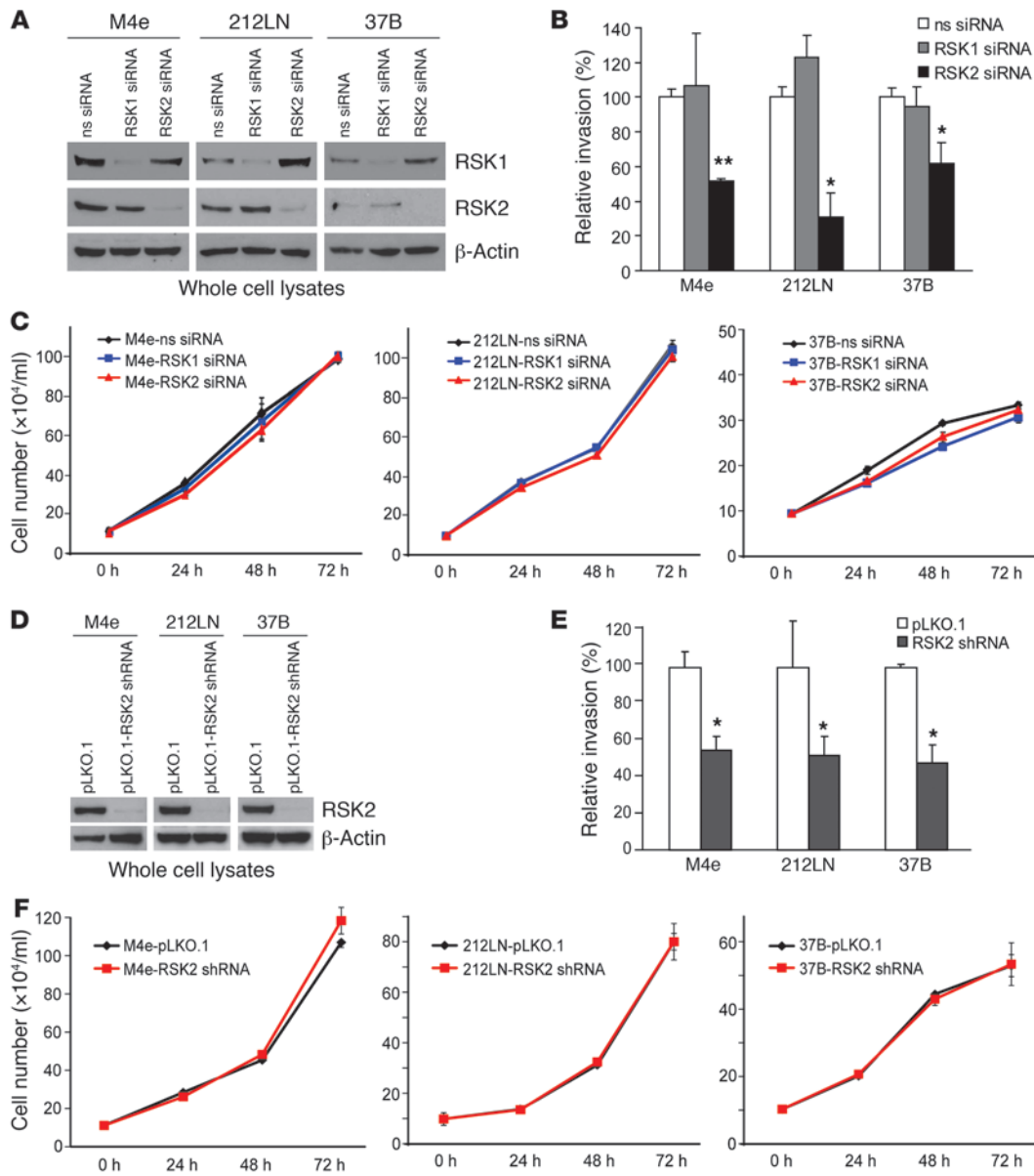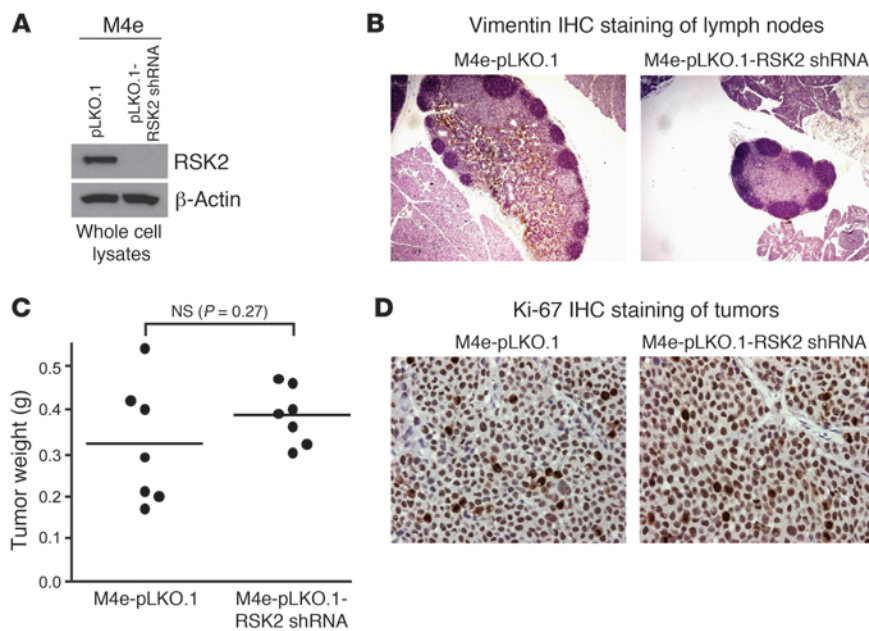
Figure 3
Targeted downregulation of RSK2 attenuates HNSCC cell invasive ability. RNAi-mediated transient (**A**) or stable (**D**) knockdown of RSK2 resulted in decreased invasive ability in RSK2-expressing HNSCC cells, including M4e, 212LN, and 37B, in the in vitro Matrigel invasion assay (**B** and **E**). Relative invasion was normalized to the invasion of control cells without RSK2 knockdown (mean ± SD). Nonsense (ns) siRNA and RSK1 siRNA were included as negative controls in **A**–**C**; M4e cells stably infected with lentivirus carrying an empty vector pLKO.1 were included as a negative control in **D**–**F**. *P = 0.01–0.05, **P < 0.01, by 2-tailed Student's t test. Transient (**C**) or stable (**F**) knockdown of RSK2 did not significantly affect the proliferation rate of M4e, 212LN, or 37B cells (mean ± SD).

nonmetastatic disease, with P values of 0.007 and less than 0.0001, respectively. Together, these results support our hypothesis that the RSK2 expression pattern correlates with human head and neck cancer metastatic progression. Positive staining of RSK2 in some cases in the group of nonmetastatic primary tumors (Tu^{-Met}) also suggests that RSK2 expression may already be positively selected for, even at the primary tumor stage prior to onset of metastasis.

RSK2 promotes cell invasion in HNSCC cells. To further substantiate the role of RSK2 in HNSCC metastasis, we next determined whether RSK2 overexpression could confer invasive potential to

the poorly invasive human HNSCC cell lines, including 686LN, Tu212, and 37A, that lack high levels of RSK2 expression. In an in vitro Matrigel invasion assay, we observed that transiently enforced RSK2 expression in these 3 independent cell lines (Figure 2A) significantly enhanced the invasive ability of these cells (Figure 2A). We then assessed the impact of targeting RSK2 on invasion of HNSCC cells. We first examined the effects of inhibiting RSK2 kinase activity by using highly specific RSK inhibitors. RSK inhibitor-fmk [RSKI-fmk; 1-(4-amino-7-(3-hydroxypropyl)-5-*p*-tolyl-7H-pyrrolo[2,3-*d*]pyrimidin-6-yl)-2-fluoroethanone] (14, 15) is a fluo-

Figure 4

RNAi-mediated stable knockdown of RSK2 significantly attenuates the metastatic potential of M4e cells in a xenograft nude mouse model. (**A**) Immunoblotting results confirm the stable knockdown of RSK2 in the M4e-pLKO.1-RSK2 shRNA cells. (**B**) Representative images of IHC staining of human vimentin in mouse LNM by M4e-pLKO.1 (brown), compared with LNs from nude mice receiving M4e-pLKO.1-RSK2 shRNA cells, to determine LNM. Original magnification, ×40. (**C**) RNAi-mediated downregulation of RSK2 did not affect tumor formation of metastatic M4e cells in vivo. Tumors from xenograft nude mice injected with control M4e-pLKO.1 cells or M4e-pLKO.1-RSK2 shRNA cells were harvested and weighed at the experimental end point. Individual points represent differential weights of tumors from distinct mice in each group. Average values are represented by horizontal bars. The P value was determined by 2-tailed Student's t test. (**D**) Representative images of IHC staining of Ki-67 (brown) from mice injected with either M4e-pLKO.1 or M4e-pLKO.1-RSK2 shRNA cells. Original magnification, ×400.

highly specific in decreasing their respective target protein expression in various HNSCC cell lines (Figure 3A). Transient transfection of RSK2-specific siRNA induced significant inhibition of invasion of M4e, 212LN, and 37B cells into matrix proteins in the Matrigel assay (Figure 3B), compared with cells transfected with nonspecific siRNA. In contrast, RSK1 siRNA failed to induce inhibition of cell invasion in these HNSCC cells (Figure 3B). Transient transfection with nonspecific RSK1 or RSK2 siRNAs did not significantly affect the proliferation rate of M4e, 212LN, and 37B cells (Figure 3C; in parallel, Western blot control is shown in Supplemental Figure 2A). These findings indicate that RSK2 but not RSK1 is involved in regulation of HNSCC cell invasion. Similar results were obtained using a lentiviral shRNA vector, pLKO.1-RSK2 shRNA, which was documented to stably reduce RSK2 protein expression by approximately 90% in distinct HNSCC cell lines (Figure 3D). Stably targeted downregulation of RSK2 using this lentiviral vector in M4e, 212LN, and 37B cells resulted in significant reduction of the invasive ability of these cells in vitro (Figure 3E) but did not significantly affect the proliferation rate of M4e, 212LN, and 37B cells (Figure 3F; in parallel, Western blot control is shown in Supplemental Figure 2B). An additional control experiment showed that stable transduction of M4e and 212LN cells with lentiviral vectors harboring scrambled shRNA or shRNA targeting GFP did not significantly affect the proliferation rate of these cells, nor did it alter the protein expression levels of RSK2 or β-actin in M4e or 212LN cells (Supplemental Figure 3 and 4).

Targeted downregulation of RSK2 by shRNA in metastatic M4e cells inhibits development of LNM in a xenograft mouse model. We next assessed the effect of knockdown of RSK2 by shRNA on the HNSCC cell metastatic potential in vivo, using a LNM xenograft mouse model (17). We used M4e cells that were demonstrated to be highly metastatic in this model (17). M4e cells, which were stably transduced with the lentiviral shRNA vector targeting RSK2 (pLKO.1-RSK2 shRNA) or an empty control vector (pLKO.1) (Figure 4A), were injected into nude mice. The mice were sacrificed on day 21, which was an endpoint determined based on our experience that M4e cells induced tumor development as well as detectable LNM in 3 weeks (data not shown). Compared with control M4e cells transduced with empty vector, M4e-pLKO.1-RSK2 shRNA cells, with stable knockdown of RSK2, showed a marked attenuation of LNM, which was characterized by the number of LNs invaded by M4e cells (Table 2), determined by IHC staining of human vimentin, a mesenchymal cell marker that is expressed in the human metastatic M4e cells but not in mouse LNs (Figure 4B).

In summary, these loss-of-function and gain-of-function studies in cells and mice support the view that continued RSK2 expression is important for maintaining the invasive and metastatic potential of HNSCC cells.

romethylketone molecule that was designed to specifically exploit 2 selectivity filters of RSK. RSKI-fmk potently inactivates the C-terminal auto-kinase domain activity of RSK1 and RSK2 with high specificity in mammalian cells (14). As shown in Figure 2B, treatment with RSKI-fmk effectively inhibited RSK2 kinase activity in 3 RSK2-expressing HNSCC cell lines, including M4e, 212LN, and 37B, as assessed by phosphorylation at Ser386, an index of RSK2 activation. Moreover, upon RSKI-fmk treatment, these cells demonstrated a significant attenuation of invasion (Figure 2, C and D). Similar results were obtained by using another RSK inhibitor, BI-D1870, which was derived from dihydropteridinones and identified as a highly specific and potent inhibitor of RSK N-terminal trans-kinase domain in kinase selectivity screening (Figure 2E) (16). Thus, targeting RSK2 by 2 distinct inhibitors, which differentially inhibit RSK2 kinase activity, results in marked reduction of HNSCC cell invasive ability. However, such decreased cell invasive ability, associated with inhibition of RSK2, was not a consequence of reduced proliferation, because treatment with either RSKI-fmk or BI-D1870 did not significantly affect the proliferation rate of M4e, 212LN, and 37B cells (Figure 2F).

We also examined the effect of RNAi-mediated RSK2 knockdown on invasion of M4e, 212LN, and 37B cells. We first used pools of siRNA specifically targeting RSK1 or RSK2 and a non-specific siRNA as a negative control. Both RSK1 and RSK2 siRNAs were

Table 2
M4e-pLKO.1-RSK2 shRNA cells, with stable knockdown of RSK2, showed a marked attenuation of LNM

	Mouse no.	Metastasis	No. of metastasized LN/ no. of LN harvested per mouse[A]
M4e-pLKO.1	476	N	0/2
	479	Y	2/3
	482	Y	2/3
	483	Y	1/2
	485	Y	4/5
	486	Y	2/2
	490	N	0/2
M4e-pLKO.1-RSK2 shRNA	498	Y	2/2
	499	N	0/2
	501	N	0/2
	502	Y	1/1
	503	N	0/2
	504	N	0/4
	505	N	0/2

Knockdown of RSK2 led to a significant reduction of LNM, characterized as the number of LNs invaded by M4e cells in the xenograft nude mice. Vimentin is a mesenchymal cell marker that is expressed in metastatic human HNSCC cells but not in mouse LNs. Positive and negative IHC staining of vimentin in LNs was indicated as yes (Y) and no (N), respectively; 3 sections of each LN were analyzed. [A]$P = 0.025$, by Fisher's exact test.

RNAi-mediated RSK2 knockdown does not attenuate proliferation and tumor formation of metastatic HNSCC cells. We next examined the possibility of whether the RSK2-dependent metastatic phenotype in vivo might be a consequence of increased proliferation. In the LNM xenograft nude mouse assay, no significant difference in the size of primary tumors was detected between the 2 groups of mice injected with either M4e-pLKO.1 or M4e-pLKO.1-RSK2 shRNA cells (Figure 4C). Moreover, stable knockdown of RSK2 in M4e-pLKO.1-RSK2 shRNA cells did not affect cell proliferation, which was assessed using the percentage of cells with positive staining of Ki-67 in each primary tumor tissue sample, when compared with control M4e-pLKO.1 cells (Table 3 and Figure 4D). Together, these in vivo data demonstrate that RSK2 possesses intrinsic prometastatic activity in HNSCC cells, which is not a consequence of enhanced proliferation.

RSK2 promotes metastasis in HNSCC cells by regulating multiple prometastatic protein factors. To explore the molecular mechanism underlying RSK2-enhanced metastasis, we surveyed potential links between RSK2 and some signaling molecules of known relevance to cell invasion and tumor metastasis. However, RNAi-mediated RSK2 knockdown in metastatic M4e cells did not affect the phosphorylation levels of ERK, AKT, and STAT3 (Figure 5A). To comprehensively find mechanistic insight into the role of RSK2 in HNSCC metastasis, we performed a phospho-proteomics–based study using a phospho-antibody microarray (Full Moon BioSystems Inc.), which provides a high-throughput platform for efficient protein phosphorylation status profiling, with detection and analysis of phosphorylation events at specific sites to identify RSK2 downstream substrates/effectors that regulate metastasis. The experiment was performed using the MAPK Pathway Phosphorylation Antibody Array, since RSK2 is a substrate of ERK.

Cell lysates obtained from M4e-pLKO.1, and M4e-pLKO.1-RSK2 shRNA cells were applied. We identified a spectrum of proteins whose phosphorylation levels were decreased more than 15%, with low values of 95% CI in M4e cells when RSK2 was stably knocked down. Many of these proteins, when phosphorylated, are important for cell migration, invasion, and tumor metastasis. These prometastatic proteins include c-Jun, CREB, Elk-1, focal adhesion kinase (FAK), Hsp27, IRS-1, JunB, c-MET, and Stathmin (Table 4 and Supplemental Table 1).

Among these proteins, we confirmed by immunoblotting that targeted downregulation of RSK2 by shRNA resulted in reduced phosphorylation and activation levels of the receptor tyrosine kinase c-MET in M4e cells and FAK in 212LN and 37B cells (Figure 5B). Although RSK2, as a serine/threonine kinase, is unlikely to directly regulate activation of these 2 prometastatic tyrosine kinases by phosphorylation, a decrease in FAK and c-MET activation upon RSK2 downregulation demonstrates the reprogramming of the HNSCC prometastatic signaling network upon RSK2 knockdown.

RSK2 phosphorylates and activates prometastatic CREB and Hsp27. To characterize the signaling properties of RSK2 in HNSCC cell invasion, we next focused on 2 potential substrates/effectors of RSK2, including a known RSK2 substrate, CREB, and Hsp27. RSK2 has been demonstrated to regulate and activate CREB by phosphorylating Ser133 (18). CREB is a transcription factor whose signaling is implicated in tumor growth and metastasis in human prostate cancer (PCa) and melanoma (19–22).

Hsp27 regulates actin dynamics (23) and has been found to be overexpressed in many human cancers. Hsp27 is regulated by phosphorylation at Ser15, Ser78, and Ser82. Phosphorylation of Hsp27 is associated with tumor cell migration and invasion and correlates with LN positivity in breast cancer (24, 25). We first determined whether RSK2 directly phosphorylates Hsp27 in an in vitro kinase assay, in which purified recombinant Hsp27 (rHsp27) WT and individual S15A, S78A, or S82A mutant proteins were incubated with active recombinant RSK2 (rRSK2). As shown in Figure 5C, the immunoblotting results using the specific phospho-Hsp27 anti-

Table 3
Stable knockdown of RSK2 in M4e cells did not attenuate cell proliferation in derived tumors

	Mouse no.	Ki-67[+] staining (%)[A]
M4e-pLKO.1[B]	476	80
	479	55
	482	85
	483	70
	485	50
	486	40
	490	45
M4e-pLKO.1-RSK2 shRNA[C]	498	75
	499	80
	501	80
	502	60
	503	40
	504	60
	505	50

IHC staining of nuclear protein Ki-67 was performed using primary tumor samples from each mouse. The percentage of cells with positive staining of Ki-67 was determined. [A]NS; $P = 0.753$, by 2-tailed Student's t test. [B]Ki-67^{+} staining average, 60.7%. [C]Ki-67^{+} staining average, 63.5%.
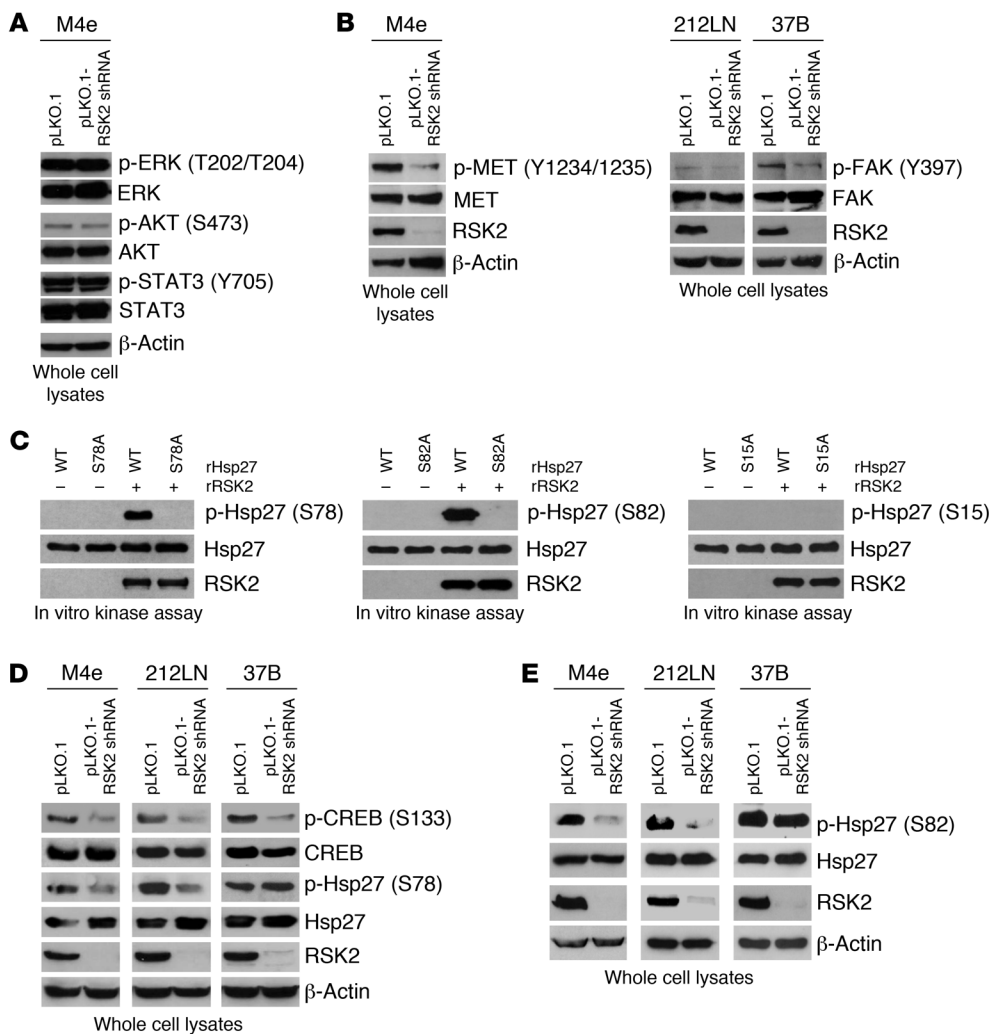
Figure 5

Targeting RSK2 by shRNA leads to decreased phosphorylation levels of multiple prometastatic protein factors, including tyrosine kinases, c-MET and FAK, and RSK2 phosphorylation substrates, CREB and Hsp27. (**A**) Stable knockdown of RSK2 did not affect phosphorylation and activation levels of ERK, AKT, and STAT3. Immunoblotting was performed using cell lysates obtained from M4e-pLKO.1 or M4e-pLKO.1-RSK2 shRNA cells. (**B**) Immunoblotting results demonstrate that targeted downregulation of RSK2 resulted in decreased tyrosine phosphorylation and activation of prometastatic tyrosine kinases c-MET in M4e cells and FAK in 212LN and 37B cells. β-actin was detected as a loading control. (**C**) RSK2 directly phosphorylated Hsp27 at S78 and S82 but not S15. Purified rHsp27 WT and individual S15A, S78A, or S82A mutant proteins were incubated with active rRSK2 in an in vitro kinase assay. Phosphorylation at Ser15, Ser78, and Ser82 in rHsp27 was detected by specific antibodies phospho-Hsp27 pS15, pS78, and pS82. (**D**) RNAi-mediated knockdown of RSK2 resulted in reduction in phosphorylation levels of CREB in RSK2-expressing M4e, 212LN, and 37B HNSCC cells and decreased Hsp27 S78 phosphorylation in M4e and 212LN cells but not 37B cells. (**E**) RNAi-mediated knockdown of RSK2 resulted in reduction in the phosphorylation level of Hsp27 S82 in M4e and 212LN cells but not 37B cells.

that to our knowledge Hsp27 is a newly identified phosphorylation substrate of RSK2.

As shown in Figure 5D, CREB S133 phosphorylation was markedly reduced in metastatic M4e, 212LN, and 37B cells upon RNAi-mediated RSK2 knockdown. Similarly, stable RSK2 knockdown in M4e and 212LN cells resulted in reduced Hsp27 S78 and S82 phosphorylation. However, RSK2 knockdown did not affect phosphorylation levels of Hsp27 S78 and S82 in 37B cells (Figure 5, D and E, respectively). Such differences may be due to disparities in the cellular contexts of distinct cell lines (discussed below).

Expression and phosphorylation levels of CREB and Hsp27 are required for RSK2-mediated pro-invasive ability of HNSCC cells. We also examined the effect of RNAi-mediated knockdown of CREB and Hsp27 on invasion of the RSK2-expressing, metastatic M4e cells. Both CREB and Hsp27 shRNAs were specific in decreasing their respective target protein expression in M4e cells (Figure 6A). Stably targeted downregulation of CREB or Hsp27, using lentiviral vectors containing distinct shRNAs in M4e cells, resulted in significant reduction of invasive ability in vitro (Figure 6B) but did not significantly affect the proliferation rate of these cells (Figure 6C).

We also found that enforced expression of RSK2 enhanced the invasive ability of Tu212 cells, whereas shRNA-mediated knockdown of CREB (Figure 6D) significantly attenuated such RSK2 expression–induced cell invasion. Moreover, stable expression of CREB WT resulted in significantly increased cell invasive ability of 686LN (Figure

6E) and Tu212 (Figure 6F) cells, and cells expressing a phospho-mimetic mutant CREB S133D demonstrated further increased cell invasive ability. In contrast, overexpressing the phospho-deficient mutant CREB S133A similarly resulted in increased cell invasion of 686LN and Tu212 cells, as did CREB WT (Figure 6, E and F, respectively), compared with control cells, but failed to further enhance the cell invasive ability like the phospho-mimetic mutants. These results suggest that expression of CREB has both S133 phosphorylation-dependent and -independent effects on HNSCC cell inva-

bodies (pS78 and pS82) demonstrate that rHsp27 WT, but not the S78A or S82A mutants, was phosphorylated at Ser78 or Ser82 by RSK2, respectively. In contrast, immunoblotting using a specific phospho-Hsp27 antibody (pS15; CST) showed that both rHsp27 WT and S15A mutant proteins were not phosphorylated at Ser15 by rRSK2 (Figure 5C). Further, in vitro kinase assays using another Hsp27 phospho-Ser15 antibody (Santa Cruz Biotechnology) and mass spectrometry–based studies confirmed that Ser15 of Hsp27 is not phosphorylated by RSK2 (data not shown). These data suggest

Table 4
Protein factors whose phosphorylation states decreased in M4e cells when RSK2 was stably knocked down by shRNA

Phosphorylation sites	Ratio (M4e-RSK2 shRNA/control)	95% CI	Prometastatic function (ref.)	RSK2 substrate
IRS-1 (p-Ser639)	0.67	0.56–0.78	41, 42	
c-Jun (p-Thr93)	0.76	0.73–0.79	43, 44	
c-Jun (p-Ser73)	0.77	0.72–0.78	43, 44	
FAK (p-Tyr861)	0.78	0.72–0.85	28, 29	
CREB (p-Ser133)	0.80	0.77–0.84	19–22	√
Hsp27 (p-Ser78)	0.81	0.77–0.86	24, 25	√
CREB (p-Ser129)	0.82	0.79–0.85	19–21	√
JunB (p-Ser79)	0.82	0.77–0.87	45	
c-Jun (p-Thr91)	0.83	0.79–0.87	43, 44	
c-MET (p-Tyr1234)	0.84	0.77–0.91	46–48	
Stathmin (p-Ser24)	0.84	0.75–0.93	49	
ER-α (p-Ser118)	0.84	0.79–0.90	50	
Elk1 (p-Thr417)	0.85	0.79–0.92	51	

The phospho-antibody microarray identified a list of protein factors whose phosphorylation states decreased in M4e cells when RSK2 was stably knocked down by shRNA. The signal intensities of phosphorylated proteins and the total protein levels were determined. The ratio of each protein was determined as the ratio between the percentages of phosphorylated proteins in total proteins in M4e-pLKO.1-RSK2 shRNA and M4e-pLKO.1 cells. 95% CI was determined to demonstrate the significance of the signal alteration for each protein factor. Tested RSK2 substrates in the current report are indicated by the √ symbol.

sion. In poorly invasive 686LN and Tu212 cells that lack high levels of RSK2 expression, only the phospho-mimetic CREB S133D, but not the phospho-deficient CREB S133A mutant, further increased cell invasive ability, compared with CREB WT. This suggests that the S133 phosphorylation-dependent pro-invasive effects of CREB depend on RSK2 expression and activation.

RSK2 promotes cell invasion by phosphorylating Hsp27 to regulate stabilization of actin filaments in HNSCC cells. Similarly, shRNA-mediated knockdown of Hsp27 significantly attenuated Tu212 cell invasion conferred by enforced expression of RSK2 (Figure 7A). Stable expression of Hsp27 WT led to increased cell invasion of poorly invasive Tu212 cells (Figure 7B) but not 686LN cells (Figure 7B). Interestingly, expression of Hsp27 phospho-mimetic mutants S78D or S82D did not lead to enhanced cell invasive capability compared with cells expressing Hsp27 WT, whereas expression of the double-mutant Hsp27 S78D/S82D significantly potentiated cell invasion of Tu212 (Figure 7B) and 686LN (Figure 7B). This result demonstrates that phosphorylation of Hsp27 at both Ser78 and Ser82 by RSK2 is crucial for its proinvasive function in HNSCC cells, while phosphorylation of Ser78 or Ser82 alone is insufficient to activate Hsp27. In contrast, overexpression of the phospho-deficient mutants Hsp27 S78A/S82A similarly resulted in increased cell invasion of 686LN and Tu212 cells to a similar degree as Hsp27 WT cells, compared with control cells, but failed to further enhance the cell invasive ability, like the phospho-mimetic mutant Hsp27 S78D/S82D (Figure 7B). Thus, these results together also implicate that Hsp27 has both S78/S82 phosphorylation-dependent and -independent effects on HNSCC cell invasion. In poorly invasive Tu212 cells that lack high expression levels of RSK2, only the phospho-mimetic double-mutant Hsp27 S78D/S82D, but not the single mutants S78D and S82D or the phospho-deficient S78A/S82A mutant, further increased cell invasive ability compared with Hsp27 WT (Figure 7B). This sug-

gests that the S78/S82 phosphorylation-dependent proinvasive effects of Hsp27 depend on RSK2 expression and activation. However, in 686LN cells, Hsp27 may only have the S78/S82 phosphorylation-dependent effect because overexpression of Hsp27 WT in these cells did not result in increased cell invasion compared with control cells (Figure 7B).

We also found that stable expression of the Hsp27 phospho-mimetic mutant S78D/S82D, but not WT or the phospho-deficient S78A/S82A mutant, partially rescued cell invasion in M4e cells with stable knockdown of RSK2 (Figure 7C). However, neither RNAi-mediated stable knockdown of RSK2 nor stable expression of Hsp27 WT, S78D/S82D, or S78A/S82A variants significantly affected the proliferation rate of M4e cells (Supplemental Figure 5).

Hsp27 has been implicated in regulation of cytoskeleton dynamics by stabilizing actin filaments (26, 27). To determine whether RSK2 regulates actin filaments, we examined the integrity of actin filaments in 212LN and M4e cells with stable knockdown of RSK2. We found that actin filaments were well organized and distributed evenly throughout the control 212LN and M4e cells transduced with empty vector. In contrast, knockdown of RSK2 induced the disruption of actin filaments and redistribution of actin to the cell membrane (Figure 7D). However, stable expression of the Hsp27 phospho-mimetic mutant S78D/S82D, but not WT or the phospho-deficient S78A/S82A mutant, rescued the formation of actin filaments in M4e cells with stable knockdown of RSK2 (Figure 7D), which correlates with rescued M4e cell invasion, as shown in Figure 7C. These data demonstrate that RSK2 regulates stabilization of actin filaments in HNSCC cells through phosphorylation of Hsp27.

Discussion
Our findings suggest that RSK2 protein expression pattern correlates with the invasive ability of diverse human HNSCC cell lines, as well as human head and neck cancer progression. Continued RSK2 expression contributes to the maintenance of the invasive and metastatic potential in HNSCC cells in vitro and in vivo, respectively. IHC study of human primary tissue samples revealed that 49% of primary tumor and 62% of LN tissue samples from patients with metastatic HNSCC were positive for RSK2 staining, which suggests that RSK2 overexpression might contribute to metastasis in a large subset of HNSCC cases. However, this finding also warrants further study to identify alternative signaling pathways that stimulate cell invasion and tumor metastasis in the RSK2-negative subset.

We also identified multiple prometastatic proteins whose phosphorylation and activation levels are regulated by RSK2 in HNSCC cells, using a phospho-antibody microarray–based proteomics approach, which has the unique capability of quantitative profiling of protein phosphorylation levels, by using paired unphospho- and phospho-antibodies for each protein. Moreover, this approach is helpful to not only identify potential substrates of particular pro-
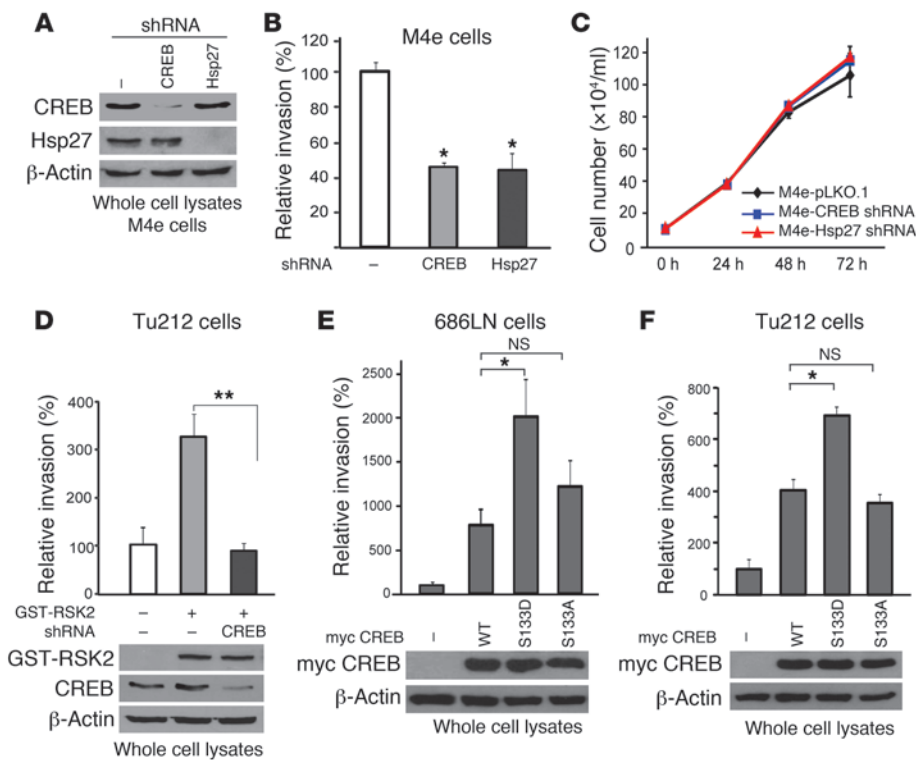
Figure 6
RSK2 promotes HNSCC cell invasion through phosphorylation and activation of the downstream substrate CREB. (**A**) RNAi-mediated stable knockdown of CREB and Hsp27 in M4e cells. (**B**) Knockdown of CREB and Hsp27 significantly reduced the invasive ability of metastatic M4e cells. Relative invasion was normalized to the invasion of M4e-pLKO.1 cells (mean ± SD; *P = 0.01–0.05). (**C**) Stable knockdown of CREB and Hsp27 did not significantly affect the proliferation rate of M4e cells (mean ± SD). (**D**) Expression of RSK2 promoted invasive ability of Tu212 cells, whereas targeted downregulation of CREB significantly attenuated RSK2-dependent invasion. Relative invasion was normalized to the invasion of control Tu212 cells (mean ± SD; **P < 0.01). (**E** and **F**) Stable expression of the phospho-mimetic CREB S133D mutant but not the phospho-deficient S133A mutant, further significantly enhanced 686LN (**E**) and Tu212 (**F**) cell invasion, compared with CREB WT. Relative invasion was normalized to the invasion of control cells harboring an empty vector (mean ± SD; *P = 0.01–0.05).

tein kinases, but also reveal connections among "remote" signaling pathways. For example, the phospho-antibody microarray–based studies revealed that phosphorylation and activation levels of 2 tyrosine kinases, c-MET and FAK, decreased upon RNAi-mediated knockdown of RSK2 in metastatic M4e cells. FAK (phospho-Y861 antibody included in the microarray) localizes at the sites of integrin clustering and cell attachment to the extracellular matrix and is central to the processes of cells migration and invasion. FAK is activated through either intrinsic autophosphorylation in response to stimuli, such as integrin engagement, or transphosphorylation by receptor tyrosine kinases (Y397) and Src family kinases (Y576, Y577, and Y861) (28, 29). Receptor tyrosine kinase c-MET proteins form heterodimers and function as receptors of HGF. Phosphorylation of Y1234/Y1235 in the juxtamembrane domain (phospho-antibodies included in the microarray) has been demonstrated to be essential for c-MET kinase activity and oncogenic potential (30, 31). Transgenic mice for either c-MET or HGF develop metastatic tumors (32), and NIH 3T3 cells overexpressing either c-MET or HGF are tumorigenic, with the derived tumors being extremely metastatic in xenograft nude mice (33). Our finding that knockdown of RSK2 resulted in decreased FAK and c-MET phosphorylation and activation suggests a crosstalk between signaling pathways involving these 2 prometastatic tyrosine kinases and the serine/threonine kinase RSK2, one which is unlikely to directly regulate phosphorylation and activation of c-MET and FAK. Therefore, our phospho-antibody microarray–based studies have paved the way for new discoveries of novel signaling pathways/crosstalk to mediate RSK2-dependent prometastatic signals and provide a fairly comprehensive view of the molecular and cellular events associated with HNSCC metastasis.

CREB is a transcription factor whose signaling is implicated in promoting tumor progression, stimulating growth, conferring apoptotic resistance, and supporting angiogenesis. In human PCa, CREB is associated with androgen-independent progression and promotes PCa bone metastasis (34). In human melanoma cells, CREB appears to be a mediator of tumor growth and metastasis, and the expression of a dominant-negative form of CREB sensitizes melanoma cells to apoptosis and inhibits their growth and metastasis (19–22). RSK2 has been implicated to regulate CREB by phosphorylating Ser133. Phosphorylation at Ser133 dictates the ability of CREB to interact with the coactivator CREB-binding protein (CBP), which mediates functional contacts with the basal transcriptional machinery (18). Our findings suggest that a transcription-dependent signaling cascade — RSK2 → CREB → prometastatic or antimetastatic genes — may be a key component of the RSK2 prometastatic signaling network in HNSCC cells.

Unlike the high-molecular-weight Hsps, Hsp70 and Hsp90, which promote protein folding, oligomerization, and translocation, Hsp27 regulates actin dynamics and apoptosis (23, 35). Hsp27 has been found to be overexpressed in breast cancer, PCa, gastric cancer, ovarian cancer, and urinary bladder cancer, and its overexpression is associated with aggressive tumor behavior and poor survival rate as well as resistance to chemotherapy (36, 37). Hsp27 activity is regulated by phosphorylation at Ser15, Ser78, and Ser82, which induces redistribution of the large oligomers into small tetrameric units (38) and Hsp27 nuclear translocation to prevent apoptosis (39). Recently, it was reported that attenuation of Hsp27 phosphorylation by the specific microtubule inhibitor KRIBB3 results in inhibition of tumor cell migration and invasion (25), while enhanced phosphorylation at Ser78 of Hsp27 significantly correlates with HER-2/neu and LN positivity in breast cancer (24). Our findings demonstrate that RSK2 signals through Hsp27 to regulate actin filaments and cell invasion via direct phosphorylation of Hsp27 at both Ser78 and Ser82 but not
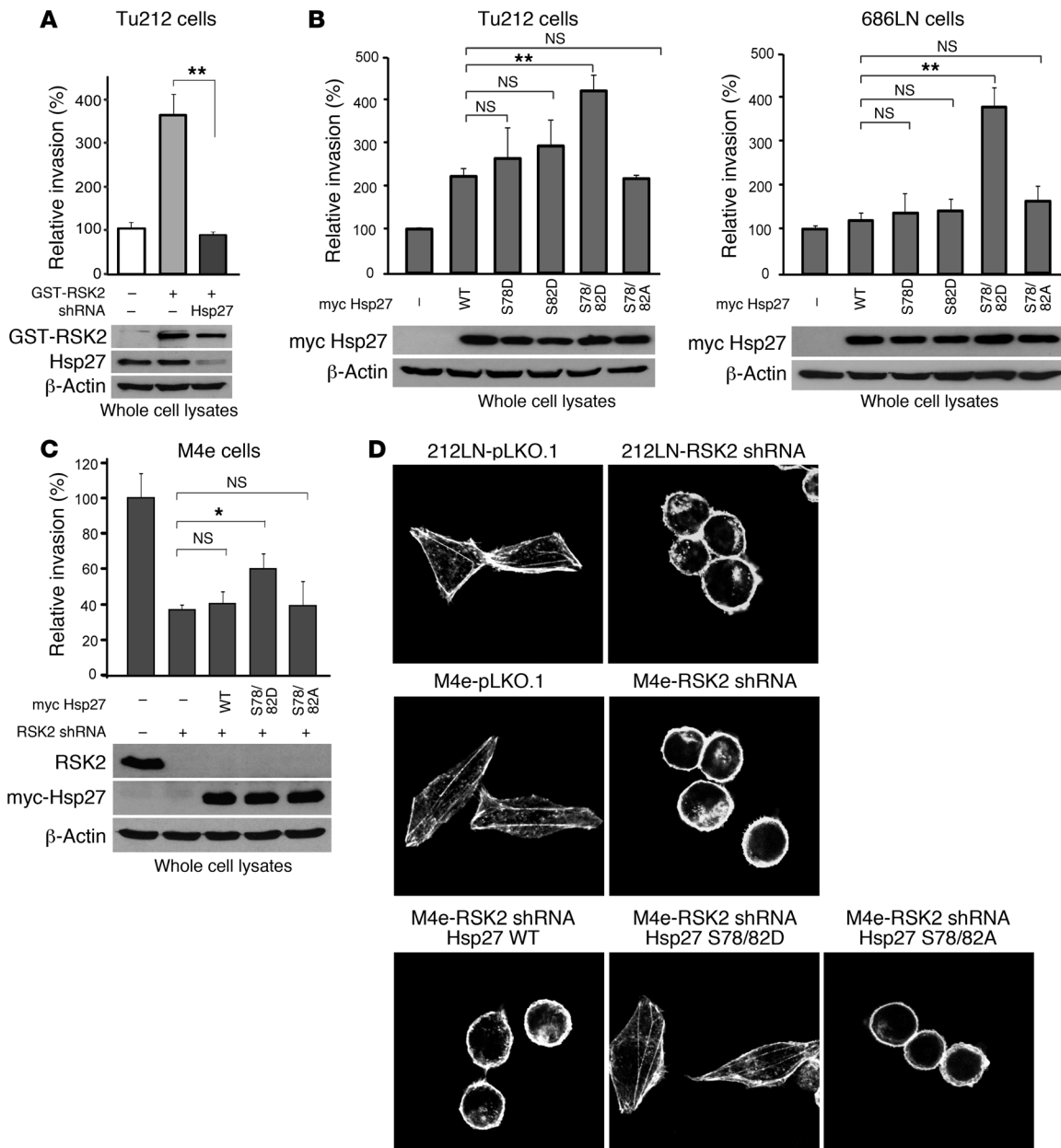
Figure 7

RSK2 promotes stabilization of actin filaments in HNSCC cells through phosphorylation and activation of Hsp27. (**A**) RNAi-mediated knockdown of Hsp27 significantly attenuated Tu212 cell invasion conferred by exogenous expression of RSK2. Relative invasion was normalized to the invasion of control Tu212 cells (mean ± SD; **$P < 0.01$). (**B**) Stable expression of the phospho-mimetic Hsp27 S78D/S82D double mutant, but not the phospho-deficient Hsp27 S78A/S82A mutant or the Hsp27 S78D and Hsp27 S82D single mutants, led to further significantly enhanced invasion of poorly invasive Tu212 and 686LN cells, compared with Hsp27 WT. Relative invasion was normalized to the invasion of control cells harboring an empty vector (mean ± SD; *$P = 0.01–0.05$; **$P < 0.01$). (**C**) Stable expression of Hsp27 S78D/S82D mutant, but not WT or S78A/S82A mutant, rescued the cell invasion attenuated by stable knockdown of RSK2 in M4e cells. Relative invasion was normalized to the invasion of M4e-pLKO.1 cells (mean ± SD; *$P = 0.01–0.05$). (**D**) Actin immunofluorescent staining shows that RNAi-mediated stable knockdown of RSK2 resulted in disruption of actin filaments in 212LN and M4e cells, whereas stable expression of the Hsp27 phospho-mimetic mutant S78D/S82D, but not WT or the phospho-deficient S78A/S82A mutant, rescued the formation of actin filaments. Cells were fixed and stained with phalloidin conjugated with Alexa Fluor 555. The integrity of actin filaments was analyzed by confocal microscopy. Original magnification, ×1,000.

Ser15. This may represent a transcription-independent mechanism underlying RSK2-mediated prometastatic signaling in HNSCC cells, in addition to the proposed transcription-dependent mechanism involving CREB.

The differential phosphorylation levels of Hsp27 in distinct metastatic HNSCC cell lines (Figure 5, D and E) indicate that each cancer cell line provides a unique platform for laboratory research. Different cellular contexts among various tumor cell lines, even those

derived from human cancer patients with the same disease symptoms and diagnosis, may require different molecular mechanisms for tumorigenesis and metastasis. Since targeting RSK2 attenuated the cell invasive ability of 37B cells, RSK2 may not signal through Hsp27 to promote cell invasion in 37B cells, as it does in M4e and 212LN cells. This also suggests that an alternative kinase or kinases may exist to phosphorylate Hsp27 S78 and S82 in 37B cells in the absence of RSK2. Interestingly, forced overexpression of either CREB WT or Hsp27 WT in poorly invasive HNSCC cells enhances cell invasion, and the phosphorylation-dependent contribution is modest compared with the effects of the nonphosphorylatable constructs in several contexts. This also suggests that different molecular mechanisms may be required by tumor cells with different cellular contexts to mediate proinvasive signals.

We recently demonstrated that targeting RSK2 by siRNA or the highly specific RSK inhibitor RSKI-fmk effectively induced apoptotic cell death in FGFR3-expressing, human t(4;14) multiple myeloma cell lines and primary patient myeloma cells, with minimal nonspecific cytotoxicity in human cells (40). These data provide proof of principle that not only suggest the therapeutic potential of targeting RSK2 in related human malignancies but also demonstrate that RSK inhibitors, such as RSKI-fmk, may have acceptable side effects. Furthermore, we found that RSK2 is more likely to be involved in HNSCC tumor metastasis than tumor initiation and growth in a xenograft mouse model (Table 2 and Figure 4). Therefore, RSK2 may represent an attractive target to attenuate tumor invasion and widespread metastasis, but not necessarily to induce regression of the primary tumor. This finding warrants the development of combined therapeutic strategies to treat metastatic HNSCC using RSK2 antagonists and other anticancer reagents that abrogate tumor growth and progression. Together, our studies not only advance the molecular understanding of tumor progression and metastasis but also inform novel therapies to treat metastatic HNSCC.

Methods

Reagents. The RSK-specific inhibitor RSKI-fmk was described previously (14, 15). BI-D1870 was purchased from the University of Dundee, Scotland, United Kingdom. siRNA was ordered from Dharmacon. Lentiviral shRNA vectors targeting RSK2, CREB, and Hsp27 were purchased from Open Biosystems. The RSK2 construct has been previously described (40). pET53-DEST-Hsp27 variants were generated for bacterial recombinant protein purification. Recombinant active RSK2 was from Invitrogen. Myc-CREB and Myc-Hsp27 variants were subcloned into retroviral vector pMSCV-hyg. Various mutants were generated using the QuikChange-XL Site-Directed Mutagenesis Kit (Stratagene).

Cell culture, lentiviral infection, retroviral infection, and proliferation assay. HNSCC Tu686 and 686LN cell lines were provided by Peter G. Sacks, New York University College of Dentistry, New York, New York. Tu212 and 212LN were provided by Gary L. Clayman, University of Texas MD Anderson Cancer Center, Houston. The 4A, 4B, 37A, and 37B cell lines were provided by Theresa L. Whiteside, University of Pittsburgh, Pennsylvania. M4e was described previously (17). All HNSCC cell lines were cultured in DMEM/Ham's F-12 50/50 mix medium in presence of 10% FBS. HNSCC cell lines stably expressing lentiviral shRNA were cultured in presence of puromycin (2 μg/ml). Lentivirus stocks carrying shRNA were generated by transfecting 293T cells with 3 μg of lentiviral vector encoding shRNA, 3 μg of pHRCMV8.2ΔR, and 0.3 μg CMV-VSVG, using Lipofectamine 2000 (Invitrogen). Forty-eight hours after transfection, supernatant harboring lentiviruses were collected. HNSCC cells were infected by lentiviruses in

6-well plates by applying infection cocktail (1 ml growing media, 0.34 ml of virus stock, and 15 μg of polybrene). After 48 hours, infected cells were selected using 2 μg/ml of puromycin for a week. Retrovirus production and retroviral infection were performed as previously described (40). For proliferation assays, 1×10^4 cells were seeded into 96-well plates, and the relative cell viability at each experimental time point was determined by using the Celltiter96AQ$_{ueous}$ One Solution Proliferation Kit (Promega). A standard curve of the cell number was generated, and the cell number of each sample was determined by normalizing the cell viability to that of the curve.

Antibodies. RSK1, RSK2, and phospho-Hsp27 (pS15) antibodies were from Santa Cruz Biotechnology; specific antibodies against phospho-RSK (S380), p44/42 ERK, phospho-p44/42 ERK (T202/T204), AKT, phospho-AKT (S473), STAT3, phospho-STAT3 (Y705), MET, phospho-MET (Y1234/Y1235), CREB, phospho-CREB (S133), Hsp27, phospho-Hsp27 (S15, S78, and S82), Myc, and FAK were from CST; phospho-FAK (Y397) was from Invitrogen; antibodies against GST and β-actin were from Sigma-Aldrich. Anti-RSK2 antibody from Novus Biologicals, prediluted anti–Ki-67 antibody from Invitrogen, and anti-human vimentin antibody from Santa Cruz Biotechnology were used for immunohistochemical staining.

Purification of rHsp27 proteins and in vitro kinase assay. (His)$_6$-tagged Hsp27 proteins were purified by sonication of BL21(DE3)pLysS cells obtained from 250 ml of culture with 0.5 mM IPTG induction for 6 hours at 25°C. Cellular lysates were resolved by centrifugation and loaded onto a Ni-NTA column (Qiagen) in 20 mM imidazole. After a step of washing twice, the protein was eluted with 250 mM imidazole. Proteins were desalted on a PD-10 column (GE Healthcare Life Sciences) and the purification efficiency was examined by Coomassie blue staining and Western blotting. To determine the ability of RSK2 to phosphorylate Hsp27, 150 ng purified recombinant (His)$_6$-Hsp27 WT and S15A, S78A, or S82A were incubated with 500 ng recombinant active RSK2 in 20 mM MOPS, 5 mM EGTA, 1 mM DTT, 25 mM β-glycerol phosphate, 1 mM Na$_3$VO$_4$, and 15 mM MgCl$_2$ along with 10 mM MgAc and 0.1 mM ATP for 30 minutes at 30°C. Phosphorylation of Ser15, Ser78, and Ser82 of Hsp27 was detected by corresponding specific phospho-antibodies.

In vitro cell invasion assay. In brief, transwell inserts with 8-μm pores (BD Biosciences) were coated with Matrigel (272 μg/ml). Approximately 2×10^5 HNSCC cells were seeded in the upper chambers in 300 μl serum-free medium, while 500 μl of medium supplemented with 10% FBS as a chemoattractant was placed in the lower wells. The chambers were incubated at 37°C in a CO$_2$ incubator. After 48 hours, the chambers were pulled out, and the noninvading cells on the upper surface were removed with the cotton swab. The cells that invaded to the lower surface of the membrane were fixed in methanol, air dried, and stained with 0.1% crystal violet for 10 minutes. The stained cells were counted in 3 random fields (at ×200 magnification) using a light microscope. The tumor cell invasion was assessed as the number of cells that had passed through the Matrigel-coated membranes.

Immunohistochemical staining. Archived, formalin-fixed, paraffin-embedded tumor specimens from HNSCC patients (prior to April 2003) that had given informed consent were identified from pathology files at the Department of Pathology and Laboratory Medicine, Emory University Hospital. Approval for use and care of these specimens was given from the Institutional Review Board of Emory University School of Medicine. Clinical information for the patients was obtained from the pathology files at Emory University Hospital under the guidelines and with approval from the Institutional Review Board of Emory University School of Medicine and according to the Health Insurance Portability and Accountability Act. Only tumors from patients that were not treated previously with either chemotherapy or radiation therapy were used. After deparaffinization and rehydration, human tissue sections were incubated in 3% hydrogen

peroxide to suppress endogenous peroxidase activity. Antigen retrieval was achieved by microwaving the sections in 100 mM Tris (pH 10.0). Sections were then blocked by incubation in 2.5% horse serum. The primary antibodies and monoclonal mouse anti-RSK2 antibody (Novus Biologicals) were applied to the slides at a dilution of 1:500 and incubated at 4°C overnight. Detection was achieved with the Avidin-Biotin Complex System (Vector Laboratories). Slides were stained with 3,3′-diaminobenzidine, washed, counterstained with hematoxylin, dehydrated, treated with xylene, and mounted. Immunohistochemical staining results were reviewed and scored as follows: 0, no staining and no background; 1+, weak cytoplasmic staining in more than 30% of cells; 2+, moderately intense cytoplasmic staining in more than 30% of cells but without intense staining in some cells; and 3+, cytoplasmic staining in more than 30% of tumor cells with markedly intense cytoplasmic staining. A similar staining procedure was performed to stain human vimentin, using LN sections of xenografted mice, and to stain Ki-67, using primary tumor tissue samples from these mice. Sodium citrate buffer (10 mM) was used for antigen retrieval, and monoclonal mouse anti-vimentin antibody was used at a dilution of 1:500 for human vimentin staining.

Xenograft nude mouse assay. Based on protocols approved by the Institutional Animal Care and Use Committee of Emory University, nude mice (athymic *nu/nu*) aged 4–6 weeks from Taconic were divided into 2 groups with similar average of weight. Each mouse was injected with 0.5×10^6 M4e-pLKO.1 or M4e-pLKO.1-RSK2 shRNA cells suspended in 50 μl of PBS into the submandibular to mylohyoid muscle as described previously (17). Tumor formation was assessed every 2–3 days. Tumor growth was recorded by measurement of 2 perpendicular diameters of the tumors over a 3-week course, using the formula $4\pi/3 \times (\text{width}/2)^2 \times (\text{length}/2)$. Mice were sacrificed 3 weeks after injection, and cervical LNs and tumors were collected, fixed immediately in 10% formalin, and embedded in paraffin. Tissue sections of LNs were stained with hematoxylin–eosin and anti-human vimentin antibody, and the primary tumor tissue sections were stained with hematoxylin–eosin and anti-RSK2 or anti-human Ki-67 antibodies. Metastases to LNs were identified by positive human vimentin staining, which is a mesenchymal cell marker that is expressed in metastatic human HNSCC cells but not in mouse LNs.

Phospho-protein profiling by phospho-antibody array. The experiment was performed by Full Moon BioSystems Inc. Cell lysates obtained from M4e-pLKO.1 and M4e-pLKO.1-RSK2 shRNA cells were applied to the MAPK Pathway Phosphorylation Antibody Array that was designed and manufactured by Full Moon Biosystems Inc. The array contains 185 antibodies, each of which has 6 replicates that are printed on standard-size coated glass microscope slides. In brief, 100 μg of cell lysates in 50 μl of reaction mixture were labeled with 1.43 μl of biotin in 10 μg/μl *N,N*-dimethylformamide. The resulting biotin-labeled proteins were diluted 1:20 in Coupling Solution (Full Moon Biosystems Inc.) before being applied to the array for conjugation. The Antibody Microarray was first blocked with blocking solution for 30 minutes at room temperature, rinsed with Milli-Q grade water for 3 minutes, and dried with compressed nitrogen, followed by incubation with the biotin-labeled cell lysates at 4°C overnight. The array slides were washed 3 times with 60 ml of 1X Wash Solution (Full Moon Biosystems Inc.) for 10 minutes each, the conjugated labeled proteins were detected using Cy3-conjugated streptavidin. For each antibody, we computed the following phosphorylation ratio (phosphorylated and matching unphosphorylated values are denoted by phospho and unphospho in both the control data and experiment data):

$$\text{phosphorylation ratio} = \frac{\text{phospho}_{\text{experiment}}}{\text{unphospho}_{\text{experiment}}} \Big/ \frac{\text{phospho}_{\text{control}}}{\text{unphospho}_{\text{control}}}$$

(Equation 1)

A 95% CI was used to quantify the precision of the phosphorylation ratio based on the analysis of the replicates. A web-based program for conducting the data analysis and generating the result table is available at http://www.mathcs.emory.edu/panda. Detailed description is available in Supplemental Methods.

Immunofluorescence staining and microscopy. For F-actin labeling, cells were seeded on glass coverslips, fixed in PHEMO buffer (68 mmol/l PIPES, 25 mmol/l HEPES, 15 mmol/l EGTA, and 3 mmol/l MgCl₂) with 3.7% formaldehyde, 0.05% glutaraldehyde, and 0.5% Triton X-100 for 10 minutes. Cells were washed in PBS and then blocked in 10% goat serum for 10 minutes. F-actin was stained for 45 minutes with Alexa Fluor 555–conjugated phalloidin (5 U/ml; Invitrogen) in PBS containing 5% goat serum. The coverslips were washed in PBS, mounted, and imaged on a Zeiss LSM 510 META confocal microscope. Confocal z-sections were acquired using a ×100 Zeiss Plan-Apo (numerical aperture, 1.4) oil objective, with identical acquisition parameters (laser intensity, gain, and zoom) in all experimental groups. The z-distance between each optical section was on average 500 nm. Images were collected in 8-bit format, with 1,024 × 1,024 resolution, and maximum projection images were created from the z-stacks. Images were exported to Adobe Photoshop, and contrast levels were expanded in all images.

Statistics. Statistical analysis and graphical presentation were done using GraphPad Prism 4.0. Data shown are from 1 experiment that is representative of multiple independent experiments and are given as mean ± SD. Statistical analysis of significance (*P* values) was based on the χ^2 test for Table 1, Fisher's exact test for Table 2, and 2-tailed Student's *t* test for all the other figures and tables. *P* values of less than 0.05 were considered significant.

Address correspondence to: Sumin Kang or Jing Chen, Winship Cancer Institute of Emory University, 1365-C Clifton Road NE, Atlanta, GA 30322. Phone: 404.778.1880; Fax: 404.778.4755; E-mail: smkang@emory.edu (S. Kang). Phone: 404.778.5274; Fax: 404.778.5520; E-mail: jchen@emory.edu (J. Chen).

1. Gupta GP, Massague J. Cancer metastasis: building a framework. *Cell*. 2006;127(4):679–695.
2. Nguyen DX, Massague J. Genetic determinants of cancer metastasis. *Nat Rev Genet*. 2007;8(5):341–352.
3. Fidler IJ. The pathogenesis of cancer metastasis: the 'seed and soil' hypothesis revisited. *Nat Rev Cancer*. 2003;3(6):453–458.
4. Haddad RI, Shin DM. Recent advances in head and neck cancer. *N Engl J Med*. 2008;359(11):1143–1154.
5. Ursini-Siegel J, Schade B, Cardiff RD, Muller WJ. Insights from transgenic mouse models of ERBB2-induced breast cancer. *Nat Rev Cancer*. 2007;

7(5):389–397.

6. Blenis J. Signal transduction via the MAP kinases: proceed at your own RSK. *Proc Natl Acad Sci U S A*. 1993;90(13):5889–5892.

7. Frodin M, Gammeltoft S. Role and regulation of 90 kDa ribosomal S6 kinase (RSK) in signal transduction. *Mol Cell Endocrinol*. 1999;151(1–2):65–77.

8. Buck M, Poli V, Hunter T, Chojkier M. C/EBPbeta phosphorylation by RSK creates a functional XEXD caspase inhibitory box critical for cell survival. *Mol Cell*. 2001;8(4):807–816.

9. He Z, Ma WY, Liu G, Zhang Y, Bode AM, Dong Z. Arsenite-induced phosphorylation of histone H3 at serine 10 is mediated by Akt1, extracellular signal-regulated kinase 2, and p90 ribosomal S6 kinase 2 but not mitogen- and stress-activated protein kinase 1. *J Biol Chem*. 2003;278(12):10588–10593.

10. Palmer A, Gavin AC, Nebreda AR. A link between MAP kinase and p34(cdc2)/cyclin B during oocyte maturation: p90(rsk) phosphorylates and inactivates the p34(cdc2) inhibitory kinase Myt1. *EMBO J*. 1998;17(17):5037–5047.

11. Shimamura A, Ballif BA, Richards SA, Blenis J. Rsk1 mediates a MEK-MAP kinase cell survival signal. *Curr Biol*. 2000;10(3):127–135.

12. Dehan E, et al. betaTrCP- and Rsk1/2-mediated degradation of BimEL inhibits apoptosis. *Mol Cell*. 2009; 33(1):109–116.

13. Anjum R, Roux PP, Ballif BA, Gygi SP, Blenis J. The tumor suppressor DAP kinase is a target of RSK-mediated survival signaling. *Curr Biol*. 2005; 15(19):1762–1767.

14. Cohen MS, Zhang C, Shokat KM, Taunton J. Structural bioinformatics-based design of selective, irreversible kinase inhibitors. *Science*. 2005; 308(5726):1318–1321.

15. Cohen MS, Hadjivassiliou H, Taunton J. A clickable inhibitor reveals context-dependent autoactivation of p90 RSK. *Nat Chem Biol*. 2007;3(3):156–160.

16. Sapkota GP, et al. BI-D1870 is a specific inhibitor of the p90 RSK (ribosomal S6 kinase) isoforms in vitro and in vivo. *Biochem J*. 2007;401(1):29–38.

17. Zhang X, et al. A lymph node metastatic mouse model reveals alterations of metastasis-related gene expression in metastatic human oral carcinoma sublines selected from a poorly metastatic parental cell line. *Cancer*. 2002;95(8):1663–1672.

18. Xing J, Ginty DD, Greenberg ME. Coupling of the RAS-MAPK pathway to gene activation by RSK2, a growth factor-regulated CREB kinase. *Science*. 1996;273(5277):959–963.

19. Jean D, Bar-Eli M. Regulation of tumor growth and metastasis of human melanoma by the CREB transcription factor family. *Mol Cell Biochem*. 2000; 212(1–2):19–28.

20. Jean D, et al. Inhibition of tumor growth and metastasis of human melanoma by intracellular anti-ATF-1 single chain Fv fragment. *Oncogene*. 2000; 19(22):2721–2730.

21. Jean D, Harbison M, McConkey DJ, Ronai Z, Bar-Eli M. CREB and its associated proteins act as survival factors for human melanoma cells. *J Biol Chem*. 1998;273(38):24884–24890.

22. Xie S, Price JE, Luca M, Jean D, Ronai Z, Bar-Eli M. Dominant-negative CREB inhibits tumor growth and metastasis of human melanoma cells. *Oncogene*. 1997;15(17):2069–2075.

23. Miron T, Vancompernolle K, Vandekerckhove J, Wilchek M, Geiger B. A 25-kD inhibitor of actin polymerization is a low molecular mass heat shock protein. *J Cell Biol*. 1991;114(2):255–261.

24. Zhang D, Wong LL, Koay ES. Phosphorylation of Ser78 of Hsp27 correlated with HER-2/neu status and lymph node positivity in breast cancer. *Mol Cancer*. 2007;6:52.

25. Shin KD, et al. Blocking tumor cell migration and invasion with biphenyl isoxazole derivative KRIBB3, a synthetic molecule that inhibits Hsp27 phosphorylation. *J Biol Chem*. 2005;280(50):41439–41448.

26. Gerthoffer WT, Gunst SJ. Invited review: focal adhesion and small heat shock proteins in the regulation of actin remodeling and contractility in smooth muscle. *J Appl Physiol*. 2001;91(2):963–972.

27. Landry J, Huot J. Modulation of actin dynamics during stress and physiological stimulation by a signaling pathway involving p38 MAP kinase and heat-shock protein 27. *Biochem Cell Biol*. 1995; 73(9–10):703–707.

28. Gabarra-Niecko V, Schaller MD, Dunty JM. FAK regulates biological processes important for the pathogenesis of cancer. *Cancer Metastasis Rev*. 2003; 22(4):359–374.

29. Mon NN, Ito S, Senga T, Hamaguchi M. FAK signaling in neoplastic disorders: a linkage between inflammation and cancer. *Ann N Y Acad Sci*. 2006; 1086:199–212.

30. Maina F, et al. Uncoupling of Grb2 from the Met receptor in vivo reveals complex roles in muscle development. *Cell*. 1996;87(3):531–542.

31. Bardelli A, et al. Uncoupling signal transducers from oncogenic MET mutants abrogates cell transformation and inhibits invasive growth. *Proc Natl Acad Sci U S A*. 1998;95(24):14379–14383.

32. Takayama H, et al. Diverse tumorigenesis associated with aberrant development in mice overexpressing hepatocyte growth factor/scatter factor. *Proc Natl Acad Sci U S A*. 1997;94(2):701–706.

33. Rong S, Segal S, Anver M, Resau JH, Vande Woude GF. Invasiveness and metastasis of NIH 3T3 cells induced by Met-hepatocyte growth factor/scatter factor autocrine stimulation. *Proc Natl Acad Sci U S A*. 1994;91(11):4731–4735.

34. Wu D, et al. cAMP-responsive element-binding protein regulates vascular endothelial growth factor expression: implication in human prostate cancer bone metastasis. *Oncogene*. 2007;26(35):5070–5077.

35. Benjamin IJ, McMillan DR. Stress (heat shock) proteins: molecular chaperones in cardiovascular

biology and disease. *Circ Res*. 1998;83(2):117–132.

36. Arrigo AP, et al. Hsp27 (HspB1) and alphaB-crystallin (HspB5) as therapeutic targets. *FEBS Lett*. 2007;581(19):3665–3674.

37. Garrido C, Brunet M, Didelot C, Zermati Y, Schmitt E, Kroemer G. Heat shock proteins 27 and 70: anti-apoptotic proteins with tumorigenic properties. *Cell Cycle*. 2006;5(22):2592–2601.

38. Lavoie JN, Lambert H, Hickey E, Weber LA, Landry J. Modulation of cellular thermoresistance and actin filament stability accompanies phosphorylation-induced changes in the oligomeric structure of heat shock protein 27. *Mol Cell Biol*. 1995;15(1):505–516.

39. Geum D, Son GH, Kim K. Phosphorylation-dependent cellular localization and thermoprotective role of heat shock protein 25 in hippocampal progenitor cells. *J Biol Chem*. 2002;277(22):19913–19921.

40. Kang S, et al. FGFR3 activates RSK2 to mediate hematopoietic transformation through tyrosine phosphorylation of RSK2 and activation of the MEK/ERK pathway. *Cancer Cell*. 2007;12(3):201–214.

41. Gibson SL, Ma Z, Shaw LM. Divergent roles for IRS-1 and IRS-2 in breast cancer metastasis. *Cell Cycle*. 2007;6(6):631–637.

42. Ma Z, Gibson SL, Byrne MA, Zhang J, White MF, Shaw LM. Suppression of insulin receptor substrate 1 (IRS-1) promotes mammary tumor metastasis. *Mol Cell Biol*. 2006;26(24):9338–9351.

43. Zhang Y, et al. c-Jun, a crucial molecule in metastasis of breast cancer and potential target for biotherapy. *Oncol Rep*. 2007;18(5):1207–1212.

44. Zhang Y, et al. Critical role of c-Jun overexpression in liver metastasis of human breast cancer xenograft model. *BMC Cancer*. 2007;7:145.

45. Robinson CM, et al. Overexpression of JunB in undifferentiated malignant rat oral keratinocytes enhances the malignant phenotype in vitro without altering cellular differentiation. *Int J Cancer*. 2001; 91(5):625–630.

46. Benvenuti S, Comoglio PM. The MET receptor tyrosine kinase in invasion and metastasis. *J Cell Physiol*. 2007;213(2):316–325.

47. Furge KA, Zhang YW, Vande Woude GF. Met receptor tyrosine kinase: enhanced signaling through adapter proteins. *Oncogene*. 2000;19(49):5582–5589.

48. Ma PC, Maulik G, Christensen J, Salgia R. c-Met: structure, functions and potential for therapeutic inhibition. *Cancer Metastasis Rev*. 2003;22(4):309–325.

49. Baldassarre G, et al. p27(Kip1)-stathmin interaction influences sarcoma cell migration and invasion. *Cancer Cell*. 2005;7(1):51–63.

50. Platet N, Cathiard AM, Gleizes M, Garcia M. Estrogens and their receptors in breast cancer progression: a dual role in cancer proliferation and invasion. *Crit Rev Oncol Hematol*. 2004;51(1):55–67.

51. Chen AG, Yu ZC, Yu XF, Cao WF, Ding F, Liu ZH. Overexpression of Ets-like protein 1 in human esophageal squamous cell carcinoma. *World J Gastroenterol*. 2006;12(48):7859–7863.